

# Bound state nature of the exotic $Z_b$ states

Martin Cleven<sup>1a</sup>, Feng-Kun Guo<sup>2b</sup>, Christoph Hanhart<sup>1c</sup>, and Ulf-G. Meißner<sup>1,2d</sup>

<sup>1</sup> Institute for Advanced Simulation and Jülich Center for Hadron Physics, Institut für Kernphysik, Forschungszentrum Jülich, D-52425 Jülich, Germany

<sup>2</sup> Helmholtz-Institut für Strahlen- und Kernphysik and Bethe Center for Theoretical Physics, Universität Bonn, D-53115 Bonn, Germany

Received: date / Revised version: date

**Abstract.** The assumption that the newly observed charged bottomonia states  $Z_b(10610)$  and  $Z_b(10650)$  are of molecular nature is confronted with the measured invariant mass distributions for the transitions of the  $\Upsilon(5S)$  to the final states  $h_b\pi^+\pi^-$  and  $h_b(2P)\pi^+\pi^-$ . It is shown that the assumption that the  $Z_b(10610)$  and  $Z_b(10650)$  are  $B\bar{B}^* + \text{c.c.}$  and  $B^*\bar{B}^*$  bound states, respectively, with very small binding energies is consistent with the data. The calculation is based on a power counting for bottom meson loops, which is explicitly given up to two-loop in the framework of a nonrelativistic effective field theory. We also show that if the  $Z_b$  states are of molecular nature, then the data should not be analyzed by using a Breit-Wigner parametrization.

**PACS.** 14.40.Rt Exotic mesons – 13.25.Gv Decays of  $J/\psi$ ,  $\Upsilon$ , and other quarkonia

## 1 Introduction

Very recently, the Belle Collaboration reported the observation of two charged bottomonia states  $Z_b(10610)$  and  $Z_b(10650)$  in five different decay channels of the  $\Upsilon(5S)$  [1]. Their masses and widths from averaging the measurements in various channels are  $M_{Z_b} = 10608.4 \pm 2.0$  MeV,  $\Gamma_{Z_b} = 15.6 \pm 2.5$  MeV, and  $M_{Z'_b} = 10653.2 \pm 1.5$  MeV,  $\Gamma_{Z'_b} = 14.4 \pm 3.2$  MeV, respectively.

The lower  $Z_b$  lies very close to the  $B\bar{B}^*$  threshold, 10604 MeV, and the higher one is close to the  $B^*\bar{B}^*$  threshold, 10650 MeV. The reported masses are slightly above the corresponding thresholds. Very soon after the discovery, it was proposed that the two  $Z_b$  states are of molecular nature [2]. To be precise, the main components in the wave functions of the  $Z_b(10610)$  and  $Z_b(10650)$  (to be called  $Z_b$  and  $Z'_b$ ) are  $B\bar{B}^* + \text{c.c.}$  and  $B^*\bar{B}^*$ , respectively. Much attention has been paid to this molecular interpretation. Calculations from QCD sum rules [3], constituent quark models [4] and one-boson-exchange model of bottom meson potentials [5] claimed the existence of  $I = 1, J^{PC} = 1^{+-}$   $B\bar{B}^*$  and  $B^*\bar{B}^*$  molecular states, and obtained masses consistent with the measured values for the two  $Z_b$  states. In Ref. [6], the authors argue that the one-pion-exchange potential does not support an  $S$ -wave  $B\bar{B}^*$  resonance state above threshold based on an effective field theory. However, as will be shown in this paper, the

experimental data in the  $h_b\pi^+\pi^-$  and  $h_b(2P)\pi^+\pi^-$  channels are also consistent with masses slightly lower than the corresponding thresholds.

As already known from many other processes and for a long time, coupled channels can produce peaks at their thresholds as a result of the unitary cut. This kind of effect was also noticed for the case of the  $Z_b$  states in [7,8,9].

In fact, the existence of an isospin vector exotic state with  $J^P = 1^+$  at the bottomonium mass region was proposed many years ago [10]. There is a long-standing puzzle in the decay  $\Upsilon(3S) \rightarrow \Upsilon(1S)\pi\pi$ . Before the measurements of the  $\pi\pi$  invariant mass spectra of the transitions from the  $\Upsilon(4S)$  to the lower-lying  $\Upsilon$  states with the emission of two pions, two evident bumps show up in the  $\pi\pi$  invariant mass spectrum of the decay  $\Upsilon(3S) \rightarrow \Upsilon(1S)\pi\pi$ , see e.g. [11]. This peculiar structure is quite different from that of the transitions  $\psi(2S) \rightarrow J/\psi\pi\pi$  and  $\Upsilon(2S) \rightarrow \Upsilon(1S)\pi\pi$ . Many models were proposed in order to resolve this puzzle. It was shown that by including the mentioned hypothetical exotic state as well as the  $\pi\pi$  final state interaction, one can describe all the data of the  $\Upsilon(nS) \rightarrow \Upsilon(mS)\pi\pi$  ( $n > m, n = 2, 3$ ) transitions well [12,13]. Later on, it was shown that the double-bump structure of the dipion invariant mass spectra of the transitions  $\Upsilon(4S) \rightarrow \Upsilon(1S, 2S)\pi\pi$  can also be described with the same exotic particle [14]. However, in all these analyses only one state was included, while the Belle Collaboration reported two  $Z_b$  states. Very recently, after the discovery of the  $Z_b$  states, they were shown to play an important role in the helicity angular distribution of the transition  $\Upsilon(5S) \rightarrow \Upsilon(2S)\pi\pi$  [15]. In all the above studies, effects

<sup>a</sup> Email address: m.cleven@fz-juelich.de

<sup>b</sup> Email address: fkguo@hiskp.uni-bonn.de

<sup>c</sup> Email address: c.hanhart@fz-juelich.de

<sup>d</sup> Email address: meissner@hiskp.uni-bonn.de

of bottom and anti-bottom meson loops which can couple to the exotic states were not taken into account. In view of the fact that these two  $Z_b$  states are in the vicinities of the  $B\bar{B}^*$  and  $B^*\bar{B}$  thresholds, respectively, the bottom meson loops could affect the line shapes of the  $Z_b$  states significantly analogous to the  $K\bar{K}$  loop effects on the  $f_0(980)$  and  $a_0(980)$  [16]. A systematic (re)analysis of all the  $\Upsilon(nS) \rightarrow \Upsilon(mS)\pi\pi$  ( $n > m, n = 2, 3, 4, 5$ ) including both  $Z_b$  states, bottom and anti-bottom meson loops and  $\pi\pi$  final state interaction is necessary [17]. In this paper, we will however focus on a simpler task, namely study the  $Z_b$  states in the decays of  $\Upsilon(5S)$  to  $h_b\pi^+\pi^-$  and  $h_b(2P)\pi^+\pi^-$  which are dominated by the  $Z_b$  states as indicated by the data [1], and check if the molecular assumption is consistent with the available experimental information. Especially we demonstrate below that the data allow for bound state poles located below the  $\bar{B}B^*$  and  $B^*\bar{B}$  thresholds, respectively.

## 2 Lagrangians

Because the spin-dependent interaction between a heavy quark and a gluon is suppressed by  $1/m_Q$ , with  $m_Q$  the heavy quark mass, in the heavy quark limit, the spin of heavy quarks decouples. Hence, it is convenient to introduce heavy hadrons and heavy quarkonia in terms of spin multiplets. In the rest frame  $v^\mu = (1, \mathbf{0})$ ,  $v$  being the heavy quark velocity, one has  $J = \mathbf{\Upsilon} \cdot \sigma + \eta_b$  with  $\mathbf{\Upsilon}$  and  $\eta_b$  annihilating the  $\Upsilon$  and  $h_b$ , respectively, and  $H_a = \mathbf{V}_a \cdot \sigma + P_a$ , with  $\mathbf{V}_a$  and  $P_a$  annihilating the vector and pseudoscalar heavy mesons, respectively.  $\sigma^i$  are the Pauli matrices, and  $a$  is the light flavor index. Explicitly, one can write  $P_a(V_a) = (B^{(*)-}, \bar{B}^{(*)0})$  for bottom mesons. The heavy mesons containing an anti-heavy quark are collected in  $\bar{H}_a = -\bar{\mathbf{V}}_a \cdot \sigma + \bar{P}_a$  [18].

The Lagrangian for the coupling of the  $\Upsilon$  to the bottom and anti-bottom mesons can be obtained by evaluating the trace in the Lagrangian

$$\mathcal{L}_\Upsilon = i\frac{g_2}{2} \left\langle J^\dagger H_a \sigma \cdot \overleftrightarrow{\partial} \bar{H}_a \right\rangle + \text{H.c.}, \quad (1)$$

where  $A \overleftrightarrow{\partial} B \equiv A(\partial B) - (\partial A)B$ . The Lagrangian for the coupling the bottom mesons to the  $P$ -wave bottomonium  $h_b$  reads [19]

$$\mathcal{L}_{h_b} = -g_1 \epsilon^{ijk} h_b^\dagger h_b^i V_a^j \bar{V}_a^k + i g_1 h_b^\dagger (V_a^i \bar{P}_a - P_a \bar{V}_a^i) + \text{H.c.} \quad (2)$$

Since the quantum numbers  $I^G(J^P) = 1^+(1^+)$  are favored for both states by the experimental analysis [1], the  $C$  parity of the neutral  $Z_b$  states should be negative. This means under parity and charge conjugation, the fields annihilating the  $Z_b$  states should transform as

$$Z^i \xrightarrow{P} Z^i, \quad Z^i \xrightarrow{C} -Z^{iT}, \quad (3)$$

and the heavy quark spin symmetry transformation is given by  $Z^i \xrightarrow{S} S Z^i \bar{S}^\dagger$  with  $S$  and  $\bar{S}$  acting on the bottom and anti-bottom quark fields, respectively. With these

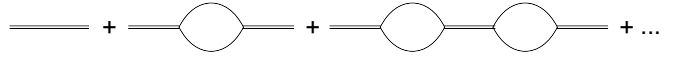


**Fig. 1.** Expansion of the two-point Green's function. Double lines and bubbles represent the bare propagators and self-energies, respectively.

transformation properties, one can construct the Lagrangian for an  $S$  wave coupling of the  $Z_b$  states to the bottom and anti-bottom mesons,

$$\mathcal{L}_Z = i\frac{z^{\text{bare}}}{2} \left\langle Z_{ba}^\dagger H_a \sigma^i \bar{H}_b \right\rangle + \text{H.c.}, \quad (4)$$

with  $z^{\text{bare}}$  is the bare coupling constant, which will be renormalized to the physical one  $z = z^{\text{bare}}\sqrt{Z}$  where  $Z$  is the wave function renormalization constant. The three different charged states are collected in a  $2 \times 2$  matrix as

$$Z_{ba}^i = \begin{pmatrix} \frac{1}{\sqrt{2}} Z^{0i} & Z^{+i} \\ Z^{-i} & -\frac{1}{\sqrt{2}} Z^{0i} \end{pmatrix}_{ba}.$$

The axial coupling of the pion fields to the heavy and anti-heavy mesons in heavy flavor chiral perturbation theory at the lowest order is given by [20,18]

$$\mathcal{L}_\pi = \frac{g}{\sqrt{2}F_\pi} \langle H_a^\dagger H_b \sigma \cdot \nabla \phi_{ba} \rangle - \frac{g}{\sqrt{2}F_\pi} \langle \bar{H}_a^\dagger \sigma \cdot \nabla \phi_{ab} \bar{H}_b \rangle. \quad (5)$$

## 3 Propagator of the $Z_b$ states

The propagator of the  $Z_b$  states is given by the two-point Green's function

$$\delta^{ij} \delta^{ab} G_Z(E) \equiv \int d^4x e^{-iEt} \langle 0 | T \{ Z_a^i(x) Z_b^{\dagger j}(0) \} | 0 \rangle, \quad (6)$$

where  $i, j$  and  $a, b$  and the indices for spin and isospin, respectively, and  $T$  denotes time order. Figure 1 illustrates the renormalization of the Green's function to one loop order. The bare propagator  $i/[2(E - \mathcal{E}_0)]$  is dressed by the self-energy  $-i\Sigma$ . Therefore, the full propagator can be written as

$$G_Z(E) = \frac{1}{2} \frac{i}{E - \mathcal{E}_0 - \Sigma(E)}. \quad (7)$$

Our convention is such that the non-relativistic normalization differs from the relativistic one by a factor of  $1/\sqrt{M_Z}$ . The self-energy in  $d$ -dimensional space-time reads

$$\Sigma(E) = i \frac{(z^{\text{bare}})^2}{4} \int \frac{d^d l}{(2\pi)^d} \frac{1}{l^0 - l^2/(2m_1) + i\epsilon} \times \frac{1}{E - l^0 - l^2/(2m_2) + i\epsilon}. \quad (8)$$

Notice that a factor of 2 has been multiplied in this definition in order to take into account both  $B\bar{B}^*$  and its charge

conjugated channel. The same factor appears in the  $B^*\bar{B}^*$  self-energy due to a different reason:  $\epsilon_{ijk}\epsilon_{i'jk} = 2\delta^{ii'}$ . In dimensional regularization with the  $\overline{\text{MS}}$  subtraction scheme, this integration is finite for  $d = 4$ . It corresponds to an implicit subtraction of the linear divergence which appears at  $d = 3$ . Taking  $d = 4$ , one has

$$\begin{aligned}\Sigma^{\overline{\text{MS}}}(E) &= (z^{\text{bare}})^2 \frac{\mu}{8\pi} \sqrt{-2\mu E - i\epsilon} \\ &= (z^{\text{bare}})^2 \frac{\mu}{8\pi} \left[ \sqrt{-2\mu E \theta(-E)} - i\sqrt{2\mu E \theta(E)} \right],\end{aligned}\quad (9)$$

where  $\mu = m_1 m_2 / (m_1 + m_2)$  is the reduced mass, and  $\theta(E) = 1$  for positive  $E$  and 0 for negative  $E$  is the step function. The superscript  $\overline{\text{MS}}$  denotes the subtraction scheme.

The bare energy  $\mathcal{E}_0$  is renormalized to the physical energy,  $\mathcal{E}$ , at the mass of the  $Z_b$ .  $\mathcal{E}$  is connected to the mass of the  $Z_b$  as  $\mathcal{E} = M_Z - m_1 - m_2$  with  $m_{1,2}$  being the masses of mesons in the loop. The renormalization condition is such that  $\mathcal{E}$  is a zero of the real part of the denominator of the propagator. Thus,  $\mathcal{E} = \mathcal{E}_0 + \text{Re}\Sigma(\mathcal{E})$ , and expanding the real part of the self-energy  $\Sigma(E)$  around  $E = \mathcal{E}$  gives

$$\begin{aligned}G_Z(E) &= \frac{1}{2} \frac{i}{(E - \mathcal{E})[1 - \text{Re}(\Sigma'(E))] - \tilde{\Sigma}(E)} \\ &= \frac{1}{2} \frac{iZ}{E - \mathcal{E} - Z\tilde{\Sigma}(E)},\end{aligned}\quad (10)$$

where the wave function renormalization constant is  $Z = [1 - \text{Re}(\Sigma'(E))]^{-1}$  with  $\Sigma'(E)$  representing the derivative of  $\Sigma(E)$  with respect to  $E$  at  $E = \mathcal{E}$ , and

$$\tilde{\Sigma}(E) = \Sigma(E) - \text{Re}(\Sigma(\mathcal{E})) - (E - \mathcal{E})\text{Re}(\Sigma'(\mathcal{E})).$$

Particularly,  $\text{Re}(\tilde{\Sigma}(\mathcal{E})) = \text{Re}(\tilde{\Sigma}'(\mathcal{E})) = 0$ . In the standard scenario (absence of nearby thresholds; stable states)  $\tilde{\Sigma}(E)$  is dropped, however, here, due to the very close branch point singularity at  $E = 0$ , this function not only acquires an imaginary part for  $E > 0$  but also varies rapidly. It therefore needs to be kept in the propagator. Eq. (10) is valid for both  $\mathcal{E} > 0$  as well as  $\mathcal{E} < 0$  (but ill defined for  $\mathcal{E} = 0$ ). The expression for  $Z$  follows from Eq. (9),

$$Z = \left[ 1 + \frac{\mu^2 (z^{\text{bare}})^2}{8\pi\gamma} \right]^{-1} \theta(-\mathcal{E}) + 1 \times \theta(\mathcal{E}).\quad (11)$$

If the  $Z_b$  ( $Z'_b$ ) is a pure  $B\bar{B}^*$  ( $B^*\bar{B}^*$ ) bound state, the wave function renormalization constant should be 0 since  $1 - Z$  measures the probability of finding a bound state in the physical state, see e.g. Refs. [21]. This means the bare coupling  $z^{\text{bare}}$  goes to infinity. However, the physical effective coupling is finite

$$(z^{\text{eff}})^2 = \lim_{|z| \rightarrow \infty} Z (z^{\text{bare}})^2 = \frac{8\pi}{\mu^2} \gamma,\quad (12)$$

with the binding momentum  $\gamma = \sqrt{-2\mu\mathcal{E}}$ . Eq. (12) coincides with the one for an  $S$  wave loosely bound state

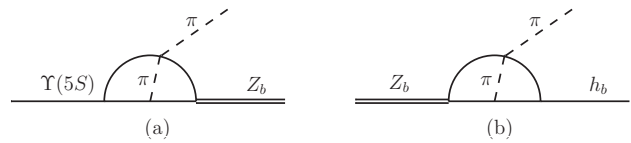


**Fig. 2.** Two loop diagrams for the subprocesses  $\Upsilon(5S) \rightarrow Z_b\pi$  (a) and  $Z_b \rightarrow h_b\pi$  (b). Solid lines in the loops represent bottom and anti-bottom mesons.

derived in Refs. [21] taking into account the factor 2 as discussed below Eq. (8).

Furthermore, the  $Z_b$  states can also decay into channels other than the bottom and anti-bottom mesons, such as  $\Upsilon(nS)\pi$  ( $n = 1, 2, 3$ ),  $h_b(1P, 2P)\pi$ ,  $\eta_b\rho$  and so on. For the complete propagator we therefore need to write

$$G_Z(E) = \frac{1}{2} \frac{iZ}{E - \mathcal{E} - Z\tilde{\Sigma}(E) + i\Gamma^{\text{phys}}(E)/2}.\quad (13)$$

According to the power counting in the non-relativistic effective field theory analyzed in details in Ref. [19], the transition amplitude between the  $Z_b$  states, which couple to the bottom mesons in an  $S$ -wave, and  $S$ -wave bottomonia should scale as  $q^2/(M_B^2 v_B)$ , with  $q$  being the external momentum, and  $v_B$  the velocity of the intermediate bottom mesons. Because  $q \ll M_B v_B^{1/2}$ , this is a suppression factor. On the other hand, the transition amplitudes to  $P$ -wave bottomonia  $h_b(1P, 2P)$  scales as  $q/v_B$ . Since  $v_B \ll 1$ , one would expect the decays from the  $Z_b$  to  $h_b(1P, 2P)\pi$  dominate those to  $\Upsilon(nS)\pi$ . Therefore we assume that  $\Gamma^{\text{phys}}$  is saturated by the former channels.

### 3.1 Power counting of two-loop diagrams

So far we have only considered one-loop diagrams. There can be more loops by exchanging pions between (anti-) bottom mesons. Following the formalism set up in Refs. [19, 22, 23], we can analyze the power counting of these higher order loops. For processes with intermediate heavy meson loops, if the virtuality of these intermediate heavy mesons is not large, their three-momenta are small compared with their masses. Hence these heavy mesons can be dealt with nonrelativistically, and one can set up a power counting in terms of the velocity of the heavy mesons,  $v_B$ . In this power counting, the momentum and energy of the intermediate mesons scale as  $v_B$  and  $v_B^2$ , respectively, and hence the measure of one-loop integration scales as  $\int d^4l \sim v_B^5$ .

There are two different topologies to be distinguished. On the one hand there are vertex corrections — those are diagrams where either one or more pions are exchanged or where a four- $B$ -meson contact operator is inserted, followed by a two-heavy meson propagator. Since the typical momentum in the loop is a lot larger than the pion mass and the pion couples with a  $P$ -wave, the vertices for the exchanged pions as well as the short ranged operator provides a factor  $v_B^\lambda$ , with  $\lambda \geq 0$ , to the power counting of the diagram. In addition, the two-loop vertex correction

has one more integral measure as well as two more propagators, each  $\sim v_B^{-2}$ . Thus in total a vertex correction appears to be suppressed by a factor  $v_B^{5+\lambda}/(v_B^2)^2 = v_B^{1+\lambda}$ . However, one needs to pay special attention to the two-loop diagrams of the kind shown in Fig. 2, where, e.g., a pion gets produced on one heavy meson and rescatters off the other one before going on-shell. These diagrams need to be analyzed case by case.

Let us first analyze the power counting of the diagram Fig. 2(a) for  $\Upsilon(5S) \rightarrow Z_b \pi$ . The leading order amplitude for the bottom meson–pion scattering formally scales as  $(E_{\pi_1} + E_{\pi_2})/F_\pi^2$ , see e.g. [26], with  $E_{\pi_{1,2}}$  the energies of the two pions. Due to some subtle cancellation mechanisms also the energy of the exchanged pion gets put on-shell in this vertex — in analogy to what happens in the reaction  $NN \rightarrow NN\pi$  [27]. For the numerical estimates below we use  $E_\pi = M_{\Upsilon(5S)} - M_{Z_b^{(\prime)}} \simeq 250$  MeV. There are two  $P$ -wave couplings in the two-loop diagrams: the coupling of the  $\Upsilon(5S)$  to the bottom and anti-bottom mesons and the vertex emitting a pion inside the loop. The  $Z_b$  bottom meson vertex is in an  $S$ -wave. The momenta from the two  $P$ -wave vertices can contract with each other, and hence scale as  $v_B^2$  (recall in the one-loop case, the  $\Upsilon(5S)B\bar{B}$   $P$ -wave vertex must contract with the external momentum, and hence scales as  $q$  [19]). There are five propagators, and each of them has a contribution of order  $v_B^{-2}$ . Therefore, the power counting of the two-loop diagram of Fig. 2(a) reads

$$\frac{(v_B^5)^2 v_B^2}{(v_B^2)^5} \frac{E_\pi}{16\pi^2 F_\pi^2} M_B = \frac{v_B^2 E_\pi M_B}{\Lambda_\chi^2}, \quad (14)$$

where the factor  $1/16\pi^2$  appears because there is one more loop compared to the one-loop case, and the chiral symmetry breaking scale is denoted as  $\Lambda_\chi = 4\pi F_\pi$ . We have introduced a factor of  $M_B$  to make the whole scaling dimensionless. One may estimate  $v_B \sim \sqrt{(\hat{M} - 2\hat{M}_B)/\hat{M}_B} \simeq 0.15$  with  $\hat{M} = (M_{\Upsilon(5S)} + M_Z)/2$  and  $\hat{M}_B$  the average mass of the bottom mesons  $B$  and  $B^*$ . This is to be compared to the one-loop diagram, which scale as  $q^2/(M_B^2 v_B)$  — see Refs. [23,19] and the previous section. Numerically, it is of similar size as or even smaller than the two-loop diagram given in Eq. (14). Hence, the two-loop diagram could be more important than the one-loop diagrams. However, the same mechanisms that suppress vertex corrections should also suppress three- or more-loop diagrams.

The situation for the transition  $Z_b \rightarrow h_b \pi$  is different. The two-loop diagram is shown in Fig. 2(b). Now there is only one  $P$ -wave vertex, which is the bottom meson–pion vertex. All the other three vertices are in an  $S$ -wave. Due to the  $P$ -wave nature of the decay  $Z_b \rightarrow h_b \pi$ , the amplitude must be proportional to the external momentum. Therefore, the only  $P$ -wave vertex should scale as  $q$ , and the product of the other three vertices scales, again, as  $E_\pi$ . Taking into account further the loop integral measure and the propagators, the power counting for this diagram reads

$$\frac{(v_B^5)^2}{(v_B^2)^5} \frac{E_\pi}{16\pi^2 F_\pi^2} q M_B = q \frac{M_B E_\pi}{\Lambda_\chi^2}, \quad (15)$$

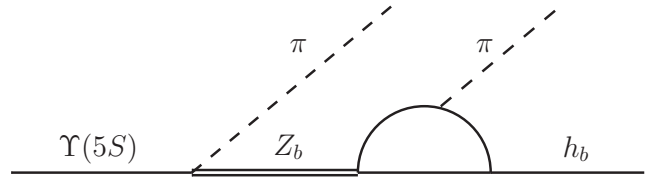


**Fig. 3.** Decay mechanism of the process  $\Upsilon(5S) \rightarrow Z_b \pi \rightarrow h_b \pi \pi$ . Solid lines in the loop represent bottom and anti-bottom mesons.

where  $M_B$  is again introduced to render the scaling dimensionless. The one-loop diagrams scale like the transitions between two  $P$ -wave heavy quarkonia. According to Ref. [19], the power counting is given by  $q/v_B$ , which is numerically much larger than the scaling for the two-loop diagram given in Eq. (15). Hence, the two-loop diagrams can be safely neglected for the  $Z_b \rightarrow h_b \pi$ .

In addition, counter-terms of the kind  $\Upsilon Z_b \pi$  need to be considered for they are needed to absorb the divergencies of the loop diagrams just discussed and are expected to be of the same importance as the loops. The corresponding Lagrangian to leading order of the chiral expansion reads

$$\mathcal{L}_{\Upsilon Z_b \pi} = c \Upsilon^i Z_{ba}^{\dagger i} \partial^0 \phi_{ab} + \text{H.c.} \quad (16)$$

The analogous counter-terms for  $Z_b h_b \pi$  can be dropped here for they are suppressed compared to the one loop diagram. Assuming the  $Z_b$  and  $Z_b^{(\prime)}$  are spin partners of each other [2], one can use the same coupling constant for them.

A full analysis would not only require the evaluation of all the diagrams mentioned above but also those where there are no  $Z_b^{(\prime)}$  present in the processes. This will be studied in a later publication [17]. Here we take a more pragmatic point of view and simply represent the whole  $\Upsilon Z_b \pi$  transition by the single contact term of Eq. (16). The full transition is illustrated in Fig. 3.

One comment is in order: the Lagrangian of Eq. (16) could as well mimic a compact component of the  $Z_b^{(\prime)}$ . This is important especially because both the two-loop and one-loop scaling given by Eq. (14) and  $q^2/(M_B^2 v_B)$  are much smaller than 1, and hence a small compact component could be more important than the bottom meson loops in the  $\Upsilon Z_b \pi$  vertex. Thus, since we expect this contact term to appear at leading order, it seems as if we would not be able to disentangle a compact, say, tetraquark component from a molecular one. However, since in the molecular scenario the transition  $Z_b \rightarrow \pi h_b$  is dominated by the loop, the structure can indeed be tested, since for molecules the dynamics appears to be quite restricted. Thus, in the present approach the  $\Upsilon(5S)\pi$  vertex provides a source term for the  $Z_b^{(\prime)}$ , while their decays are the subject of this study.

## 4 Results

The relevant vertices follow from these Lagrangians. The decay amplitudes for the two-body transitions can be found in Appendix A. On one hand, the  $\Upsilon(5S)$  is only about 120 and 70 MeV above the  $Z_b\pi$  and  $Z'_b\pi$  thresholds, respectively. On the other hand, it has a large width  $110 \pm 13$  MeV, and the experimental data were taken in an energy range around the  $\Upsilon(5S)$  mass. Therefore, when calculating its decay widths, one has to take into account the mass distribution of the  $\Upsilon(5S)$ . Its three-body decay width can then be calculated using

$$\Gamma(\Upsilon(5S))_{3\text{-body}} = \frac{1}{W} \int_{(M_\Upsilon - 2\Gamma_\Upsilon)^2}^{(M_\Upsilon + 2\Gamma_\Upsilon)^2} ds \frac{(2\pi)^4}{2\sqrt{s}} \int d\Phi_3 |\mathcal{A}|^2 \times \frac{1}{\pi} \text{Im} \left( \frac{-1}{s - M_\Upsilon^2 + iM_\Upsilon\Gamma_\Upsilon} \right), \quad (17)$$

where  $M_\Upsilon = 10.865$  GeV and  $\Gamma_\Upsilon = 0.11$  GeV are the mass and width of the  $\Upsilon(5S)$ , respectively, and  $\int d\Phi_3$  denotes the three-body phase space, see e.g. [24]. The function  $\mathcal{A}$  contains all the physics and can be easily obtained using the loop amplitudes given explicitly in the appendix. Both positively and negatively charged  $Z_b$  and  $Z'_b$  states should be considered. The factor  $1/W$  with

$$W = \int_{(M_\Upsilon - 2\Gamma_\Upsilon)^2}^{(M_\Upsilon + 2\Gamma_\Upsilon)^2} ds \frac{1}{\pi} \text{Im} \left( \frac{-1}{s - M_\Upsilon^2 + iM_\Upsilon\Gamma_\Upsilon} \right)$$

is considered in order to normalize the spectral function of the  $\Upsilon(5S)$ .

We consider the case that the  $Z_b$  and  $Z'_b$  couple only to the  $B\bar{B}^* + \text{c.c.}$  and  $B^*\bar{B}$  channels, respectively. Coupled channel effects should be suppressed because  $|\mathcal{E}| \ll M_{B^*} - M_B$  for both  $Z_b$  states.

The parameters of the model are the normalization factors  $N$ , chosen individually for the two final states, the physical couplings, which are products of  $\sqrt{Z}$  and the bare couplings, for the  $Z_b$  states to the relevant open bottom channels,  $z_1$  and  $z_2$  (or equivalently the binding energies of the  $Z_b^{(\prime)}$ ), and those couplings for the  $h_b$  and  $h_b(2P)$ , denoted by  $g_1$  and  $g'_1$ , respectively. The parameter  $c$  of Eq. (16) is absorbed into the overall normalization factor. Both  $g_1$  and  $g'_1$  only appear in a product with the  $z_i$ . In order to reduce the number of free parameters, we assume  $g'_1 = g_1$  in the following. Note that neither of them can be measured directly, since the masses of  $h_b$  and  $h_b(2P)$  are below the  $\bar{B}B^*$  threshold. In the actual fit we will adjust  $z_1$ ,  $r_z \equiv z_2/z_1$ ,  $g_1 z_1$  and the two normalization constants.

Using the amplitudes of Eqs. (A.2,A.3), we fit the parameters to the invariant mass spectra of both  $h_b\pi^+$  and  $h_b(2P)\pi^+$  from 10.56 GeV to 10.70 GeV in the missing mass spectrum  $MM(\pi)$ . In the chosen region, there are 14 data points for the  $\Upsilon(5S) \rightarrow h_b\pi^+\pi^-$  and 13 for the  $\Upsilon(5S) \rightarrow h_b(2P)\pi^+\pi^-$ .

The decay widths of the  $Z_b$  and  $Z'_b$  into  $h_b\pi$  are obtained to be

$$\begin{aligned} \Gamma(Z_b \rightarrow h_b\pi) &= 4.8 \left( \frac{gg_1 z_1}{F_\pi} \text{GeV}^2 \right)^2 \text{ MeV} \\ &= 140(g_1 z_1 \text{GeV})^2 \text{ MeV}, \\ \Gamma(Z'_b \rightarrow h_b\pi) &= 5.8 \left( \frac{gg_1 z_2}{F_\pi} \text{GeV}^2 \right)^2 \text{ MeV} \\ &= 169(g_1 z_2 \text{GeV})^2 \text{ MeV}. \end{aligned} \quad (18)$$

Due to smaller phase space, the widths for the decays  $Z_b^{(\prime)} \rightarrow h_b(2P)\pi$  get smaller numerical factors. We find

$$\begin{aligned} \Gamma(Z_b \rightarrow h_b(2P)\pi) &= 30(g'_1 z_1 \text{GeV})^2 \text{ MeV}, \\ \Gamma(Z'_b \rightarrow h_b(2P)\pi) &= 46(g'_1 z_2 \text{GeV})^2 \text{ MeV}. \end{aligned} \quad (19)$$

In getting the above numbers, we use  $F_\pi = 92.4$  MeV. Because the  $B^*$  is below the  $B\pi$  threshold, the axial coupling constant  $g$  cannot be directly measured. Fortunately, there have been quite a few theoretical determinations using different methods. For a collection of these results, see [25]. Almost all the determinations fall in the range between 0.3 and 0.7, and  $g = 0.5$  is used here.

If the  $Z_b$  and  $Z'_b$  states are  $S$ -wave bound states of the  $B\bar{B}^*$  and  $B^*\bar{B}$ , respectively, their coupling strengths to the bottom and anti-bottom mesons are related to the binding energies. The relation has been derived in Eq. (12). The coupling constants  $z_i$  appear in Eqs. (18), which enter the  $Z_b$  propagators, as well as in the transition amplitudes — c.f. Eqs. (A.2,A.3).

In order to fit to the data which are events collected per 10 MeV, we integrate the invariant mass spectra for each bin corresponding to the measurements. This is important for narrow structures. The best fit results in  $\chi^2/\text{d.o.f.} = 54.1/22 = 2.45$ .

$$\begin{aligned} z_1 &= 0.75_{-0.11}^{+0.08} \text{ GeV}^{-1/2}, & r_z &= -0.39_{-0.07}^{+0.06}, \\ g_1 z_1 &= 0.40 \pm 0.06 \text{ GeV}^{-1}. \end{aligned} \quad (20)$$

The results from the best fit are plotted in Fig. 4 together with the experimental data. Using Eq. (12) the couplings can be converted to binding energies. Especially we find

$$\mathcal{E}_{Z_b} = -4.7_{-2.3}^{+2.2} \text{ MeV}, \quad \mathcal{E}_{Z'_b} = -0.11_{-0.14}^{+0.06} \text{ MeV}. \quad (21)$$

Although the  $Z_b$  and  $Z'_b$  are supposedly spin partners, a value of  $r_z = -0.4$  is not completely unreasonable: the fine tuning necessary to put a bound state as close as 0.1 MeV to a threshold is extremely sensitive to even a small variation in the scattering potential, driven by spin symmetry violations. In effect this can give significant differences in the binding energies and, via Eq. (12), also in the coupling constants. However, a microscopic calculation, which goes beyond the scope of this paper, would be necessary to check this hypothesis.

One can obtain a better fit to the data if one would either release the bound state condition given as Eq. (12), and allowing the masses of the  $Z_b$  states to float freely, or

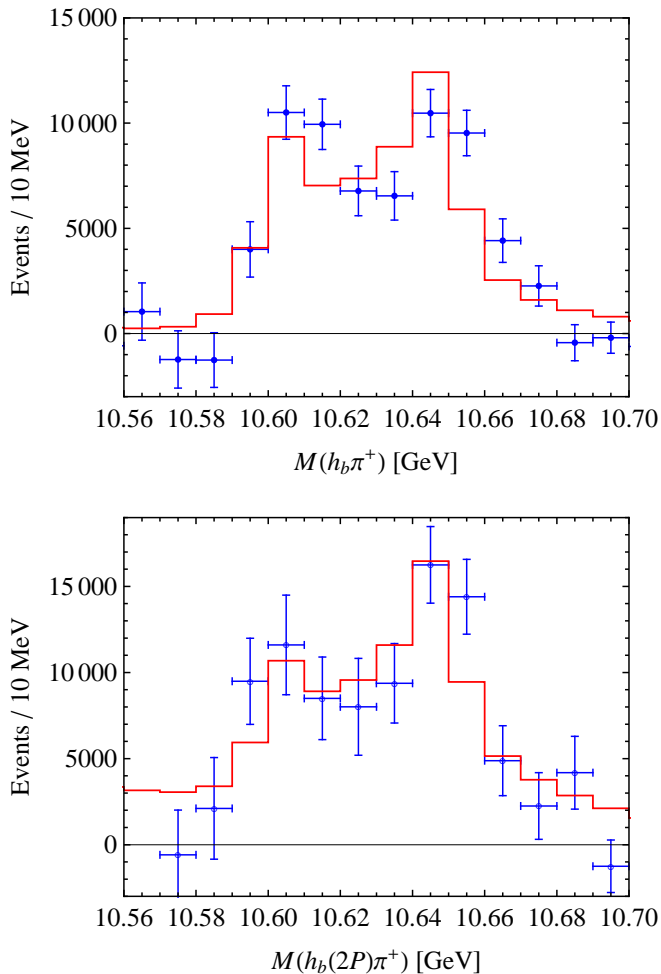


**Fig. 4.** Comparison of the calculated invariant mass spectra of  $h_b\pi^+$  and  $h_b(2P)\pi^+$  with the measured missing mass spectra  $MM(\pi)$ .

allow for non-resonant terms. But this is not the purpose of our paper — we here only want to demonstrate that the data are consistent with the bound state picture, which implies the masses of the  $Z_b^{(\prime)}$  states to be located below the corresponding thresholds.

It is interesting to look at the  $Z_b$  line shape or the absolute value of  $G_Z(E)$  for different locations of the  $Z_b$  pole. The function  $|G_Z(E)|$  using the parameters from the best fit are plotted as the solid line in Fig. 5. In this case, the  $Z_b$  is a  $B\bar{B}^*$  bound state with a binding energy of  $-4.7$  MeV. Keeping  $z_1 = 0.75$  GeV $^{-1/2}$ , and  $g_1 z_1 = 0.4$  GeV $^{-1}$  fixed we also plot as the dashed line the line shape for the virtual state with the same value of  $\mathcal{E}$ .<sup>1</sup> The dotted and dot-dashed lines are for a resonance with a mass above the  $B\bar{B}^*$  threshold by 8 and 20 MeV, respectively. From the figure, one sees that the bound state produces a bump be-

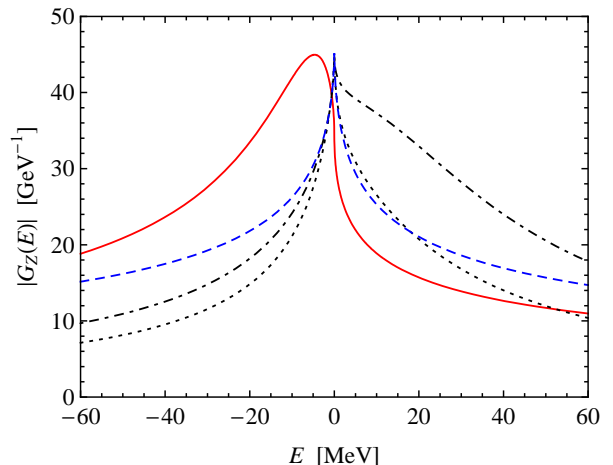


**Fig. 5.** The absolute value of  $G_Z(E)$ . The solid (red) and dashed (blue) are for a bound state and virtual state, respectively, with the same mass,  $\mathcal{E} = M_{Z_b} - M_B - M_{B^*} = -4.7$  MeV. The dotted and dot-dashed (black) lines are for resonances with  $\mathcal{E} = 8$  and 20 MeV, respectively. The maxima of the resonance and virtual state curves have been normalized to the bound state one.

low the threshold, and a small cusp at the threshold, while the virtual state produces a prominent cusp at the threshold and no structure below. Above the threshold, the energy dependence of the virtual and bound state curves are exactly the same. The bump in the bound state case reflects the pole position. Hence, if we reduce the value of binding energy to, say about 0.1 MeV, which is the case for the  $Z_b'$  and the  $X(3872)$ , then the bump below threshold would be invisible, and the cusp dominates the structure. In this case, it is hard to distinguish between the bound state and virtual state scenarios. For more discussions on the shape of a virtual state, see e.g. [28,29].

One important feature of the line shapes of dynamically generated states is shown in Fig. 5: for poles slightly above the threshold, since the coupling to the opening channel is strong, the position of the peak is *locked to the threshold*, as can be seen from the dotted line. Increasing the resonance mass, the effect of the cusp is smeared out, and shape is approaching a normal Breit-Wigner resonance — in the dot-dashed line one starts to see a bump above threshold developing for a mass as large as 20 MeV above the  $B\bar{B}^*$  threshold. However, even then the peak is still located at the threshold. We are therefore to conclude that a Breit-Wigner parametrization, as was used in the experimental analysis, should not be used when analyzing structures that emerge from dynamically generated states.

## 5 Conclusion

We showed that the data [1] is consistent with the assumption that the main components of the lower and higher  $Z_b$  states are  $S$ -wave  $B\bar{B}^* + \text{c.c.}$  and  $B^*\bar{B}^*$  bound states, respectively. A small compact tetraquark component, however, can not be excluded.

<sup>1</sup> The curve for virtual state is obtained using Eq. (10) but with  $\tilde{\Sigma}(E) = \Sigma(E) - \text{Re}(\Sigma_{\text{II}}(\mathcal{E})) - (E - \mathcal{E})\text{Re}(\Sigma'(\mathcal{E}))$ , where, in the  $\overline{\text{MS}}$  scheme,  $\text{Re}(\Sigma_{\text{II}}(\mathcal{E})) = -\text{Re}(\Sigma(\mathcal{E}))$  is the self-energy in the second Riemann sheet.

It is difficult to distinguish between resonance and bound state scenarios with the current data, however, data with higher resolution should allow one to distinguish the two cases — see, e.g., Refs. [30,31] for the corresponding discussion for the  $X(3872)$ . In a next step we will improve the model by inclusion of non-resonant terms as well as the calculation of other decay channels [17].

We have demonstrated that if the  $Z_b$  states are indeed generated from non-perturbative  $B\bar{B}^* + \text{c.c.}$  and  $B^*\bar{B}$  dynamics, the data should not be analyzed using a Breit-Wigner parametrization. This statement can also be reversed: if a near threshold state can be described by a Breit-Wigner form, it is not dynamically generated, as this is possible only if the coupling of the resonance to the continuum channel is very weak. At present the data appears to be consistent with line shapes that result from dynamical states as well as genuine ones. Therefore a decision about the nature of the  $Z_b$  states will be possible only once data with higher resolution and statistics will be available.

## Acknowledgments

We thank the HGF for funds provided to the virtual institute “Spin and strong QCD” (VH-VI-231), the DFG (SFB/TR 16) and the EU I3HP “Study of Strongly Interacting Matter” under the Seventh Framework Program of the EU. U.-G. M. also thanks the BMBF for support (Grant No. 06BN9006).

## A Loop function and expressions of the amplitudes

The basic three-point loop function worked out using dimensional regularization in  $d = 4$  is

$$\begin{aligned}
& I(m_1, m_2, m_3, \mathbf{q}) \\
&= \frac{-i}{8} \int \frac{d^d l}{(2\pi)^d} \frac{1}{\left(l^0 - \frac{l^2}{m_1} + i\epsilon\right)} \frac{1}{\left(l^0 + b_{12} + \frac{l^2}{m_2} - i\epsilon\right)} \\
&\quad \times \frac{1}{\left[l^0 + b_{12} - b_{23} - \frac{(l-\mathbf{q})^2}{m_3} + i\epsilon\right]} \\
&= \frac{\mu_{12}\mu_{23}}{16\pi} \frac{1}{\sqrt{a}} \left[ \tan^{-1} \left( \frac{c' - c}{2\sqrt{a(c - i\epsilon)}} \right) \right. \\
&\quad \left. + \tan^{-1} \left( \frac{2a + c - c'}{2\sqrt{a(c' - a - i\epsilon)}} \right) \right], \tag{A.1}
\end{aligned}$$

where  $m_i (i = 1, 2, 3)$  are the masses of the particles in the loop,  $\mu_{ij} = m_i m_j / (m_i + m_j)$  are the reduced masses,  $b_{12} = m_1 + m_2 - M$ ,  $b_{23} = m_2 + m_3 + q^0 - M$  with  $M$  the mass of the initial particle, and

$$a = \left( \frac{\mu_{23}}{m_3} \right)^2 \mathbf{q}^2, \quad c = 2\mu_{12}b_{12}, \quad c' = 2\mu_{23}b_{23} + \frac{\mu_{23}}{m_3} \mathbf{q}^2.$$

For more information about the loop function, we refer to Appendix A in Ref. [19]. Note that different from the convention of Ref. [19], here the factor  $1/(m_1 m_2 m_3)$  has been dropped.

In terms of the loop function given above, the amplitudes for  $Z_b^+$  and  $Z_b'^+$  decays into  $h_b \pi^+$  are

$$\begin{aligned}
\mathcal{A}_{Z_b^+ h_b} &= \frac{2\sqrt{2}gg_1z_1}{F_\pi} \sqrt{M_{h_b} M_{Z_b}} \epsilon_{ijk} q^i \epsilon_{Z_b}^j \epsilon_{h_b}^k \\
&\quad \times [I(M_B, M_{B^*}, M_{B^*}, \mathbf{q}) + I(M_{B^*}, M_B, M_{B^*}, \mathbf{q})], \tag{A.2}
\end{aligned}$$

and

$$\begin{aligned}
\mathcal{A}_{Z_b'^+ h_b} &= \frac{2\sqrt{2}gg_1z_2}{F_\pi} \sqrt{M_{h_b} M_{Z_b'}} \epsilon_{ijk} q^i \epsilon_{Z_b'}^j \epsilon_{h_b}^k \\
&\quad \times [I(M_{B^*}, M_{B^*}, M_B, \mathbf{q}) + I(M_{B^*}, M_{B^*}, M_{B^*}, \mathbf{q})], \tag{A.3}
\end{aligned}$$

respectively. In all these amplitudes, both the neutral and charged bottom and anti-bottom mesons have been taken into account.

## References

1. I. Adachi et al. [Belle Collaboration], arXiv:1105.4583 [hep-ex].
2. A. E. Bondar, A. Garmash, A. I. Milstein, R. Mizuk and M. B. Voloshin, arXiv:1105.4473 [hep-ph].
3. J. R. Zhang, M. Zhong and M. Q. Huang, arXiv:1105.5472 [hep-ph].
4. Y. Yang, J. Ping, C. Deng and H. S. Zong, arXiv:1105.5935 [hep-ph].
5. Z. F. Sun, J. He, X. Liu, Z. G. Luo and S. L. Zhu, arXiv:1106.2968 [hep-ph].
6. J. Nieves and M. P. Valderrama, arXiv:1106.0600 [hep-ph].
7. D. V. Bugg, arXiv:1105.5492 [hep-ph].
8. I. V. Danilkin, V. D. Orlovsky and Yu. A. Simonov, arXiv:1106.1552 [hep-ph].
9. D. Y. Chen and X. Liu, arXiv:1106.3798 [hep-ph].
10. M. B. Voloshin, JETP Lett. **37**, 69 (1983) [Pisma Zh. Eksp. Teor. Fiz. **37**, 58 (1983)].
11. F. Butler *et al.* [CLEO Collaboration], Phys. Rev. D **49**, 40(1994).
12. V. V. Anisovich, D. V. Bugg, A. V. Sarantsev and B. S. Zou, Phys. Rev. D **51**, 4619 (1995).
13. F. K. Guo, P. N. Shen, H. C. Chiang and R. G. Ping, Nucl. Phys. A **761**, 269 (2005) [arXiv:hep-ph/0410204].
14. F. K. Guo, P. N. Shen, H. C. Chiang and R. G. Ping, Phys. Lett. B **658**, 27 (2007) [arXiv:hep-ph/0601120].
15. D. Y. Chen, X. Liu and S. L. Zhu, arXiv:1105.5193 [hep-ph].
16. S. M. Flatté, Phys. Lett. B **63**, 224 (1976).
17. M. Cleven, F. K. Guo, C. Hanhart and U.-G. Meißner, in preparation.
18. S. Fleming, T. Mehen, Phys. Rev. D **78**, 094019 (2008). [arXiv:0807.2674 [hep-ph]].
19. F. K. Guo, C. Hanhart, G. Li, U.-G. Meißner and Q. Zhao, Phys. Rev. D **83**, 034013 (2011) [arXiv:1008.3632 [hep-ph]].

20. G. Burdman and J. F. Donoghue, *Phys. Lett. B* **280**, 287 (1992); M. B. Wise, *Phys. Rev. D* **45**, R2188 (1992); T. M. Yan, H. Y. Cheng, C. Y. Cheung, G. L. Lin, Y. C. Lin and H. L. Yu, *Phys. Rev. D* **46**, 1148 (1992) [Erratum-ibid. *D* **55**, 5851 (1997)]; R. Casalbuoni, A. Deandrea, N. Di Bartolomeo, R. Gatto, F. Feruglio and G. Nardulli, *Phys. Rept.* **281**, 145 (1997) [arXiv:hep-ph/9605342].
21. S. Weinberg, *Phys. Rev.* **130**, 776 (1963); *Phys. Rev.* **131**, 440 (1963); *Phys. Rev.* **137**, B672 (1965); V. Baru, J. Haidenbauer, C. Hanhart, Yu. Kalashnikova and A. E. Kudryavtsev, *Phys. Lett. B* **586**, 53 (2004) [arXiv:hep-ph/0308129].
22. F. K. Guo, C. Hanhart and U.-G. Meißner, *Phys. Rev. Lett.* **103**, 082003 (2009) [Erratum-ibid. **104**, 109901 (2010)] [arXiv:0907.0521 [hep-ph]].
23. F. K. Guo, C. Hanhart, G. Li, U.-G. Meißner and Q. Zhao, *Phys. Rev. D* **82**, 034025 (2010) [arXiv:1002.2712 [hep-ph]].
24. K. Nakamura *et al.* [Particle Data Group], *J. Phys. G* **37**, 075021 (2010).
25. X. Q. Li, F. Su and Y. D. Yang, *Phys. Rev. D* **83**, 054019 (2011) [arXiv:1011.0269 [hep-ph]].
26. F. K. Guo, C. Hanhart and U.-G. Meißner, *Eur. Phys. J. A* **40**, 171 (2009) [arXiv:0901.1597 [hep-ph]].
27. V. Lensky, V. Baru, J. Haidenbauer, C. Hanhart, A. E. Kudryavtsev, U.-G. Meißner, *Eur. Phys. J. A* **27**, 37 (2006) [nucl-th/0511054].
28. K. W. McVoy, *Nucl. Phys.* **A115**, 481 (1968).
29. V. Baru, J. Haidenbauer, C. Hanhart, A. E. Kudryavtsev, U.-G. Meißner, *Eur. Phys. J. A* **23**, 523 (2005) [nucl-th/0410099].
30. C. Hanhart, Y. S. Kalashnikova, A. E. Kudryavtsev, A. V. Nefediev, *Phys. Rev. D* **76**, 034007 (2007) [arXiv:0704.0605 [hep-ph]].
31. E. Braaten, M. Lu, *Phys. Rev. D* **76**, 094028 (2007) [arXiv:0709.2697 [hep-ph]].